Secondary neutron dose contribution from pencil beam scanning, scattered and spatially fractionated proton therapy

Amélia Maia Leite, Maria Crazia Ronga, Maria Giorgi, Yoann Ristic, Yann Perrot, Francois Trompier, Yolanda Prezado, Gilles Crehange, Ludovic de Marzi

▶ **To cite this version:**

Amélia Maia Leite, Maria Crazia Ronga, Maria Giorgi, Yoann Ristic, Yann Perrot, et al.. Secondary neutron dose contribution from pencil beam scanning, scattered and spatially fractionated proton therapy. Physics in Medicine and Biology, 2021, 66, pp.225010. 10.1088/1361-6560/ac3209 . hal-03546321

HAL Id: hal-03546321
https://hal.science/hal-03546321

Submitted on 27 Jan 2022

HAL is a multi-disciplinary open access archive for the deposit and dissemination of scientific research documents, whether they are published or not. The documents may come from teaching and research institutions in France or abroad, or from public or private research centers.

L'archive ouverte pluridisciplinaire **HAL**, est destinée au dépôt et à la diffusion de documents scientifiques de niveau recherche, publiés ou non, émanant des établissements d'enseignement et de recherche français ou étrangers, des laboratoires publics ou privés.

Secondary neutron dose contribution from pencil beam scanning, scattered and spatially fractionated proton therapy

A.M.M. Leite[1,2*], M.G. Ronga[1], M. Giorgi[1], Y. Ristic[3], Y. Perrot[3], F. Trompier[3], Y. Prezado[2], G. Créhange[1] and L. De Marzi[1,4*]

[1] Institut Curie, PSL Research University, Radiation Oncology Department, Proton Therapy Centre, Centre Universitaire, 91898 Orsay, France
[2] Institut Curie, PSL Research University, University Paris Saclay, Inserm U 1021- CNRS UMR 3347, 91898, Orsay, France
[3] Institut de Radioprotection et de Sûreté Nucléaire, Service de Dosimétrie, Laboratoire de Dosimétrie des Rayonnements Ionisants, 92262 Fontenay-aux-Roses Cedex, France
[4] Institut Curie, PSL Research University, University Paris Saclay, Inserm LITO, 91898 Orsay, France

E-mail: amelia.maialeite@curie.fr, ludovic.demarzi@curie.fr

Abstract

The Orsay Proton therapy Center (ICPO) has a long history of intracranial radiotherapy using both double scattering (DS) and pencil beam scanning (PBS) techniques, and is actively investigating a promising modality of spatially fractionated radiotherapy using proton minibeams (pMBRT). This work provides a comprehensive comparison of the organ-specific secondary neutron dose due to each of these treatment modalities, assessed using Monte Carlo (MC) algorithms and measurements.

A MC model of a universal nozzle was benchmarked by comparing the neutron ambient dose equivalent, H*(10), in the gantry room with measurements obtained using a WENDI—II counter. The secondary neutron dose was evaluated for clinically relevant intracranial treatments of patients of different ages, in which secondary neutron doses were scored in anthropomorphic phantoms merged with the patients' images.

The MC calculated H*(10) values showed a reasonable agreement with the measurements and followed the expected tendency, in which PBS yields the lowest dose, followed by pMBRT and DS. Our results for intracranial treatments show that pMBRT yielded a higher secondary neutron dose for organs closer to the target volume, while organs situated furthest from the target volume received a greater quantity of neutrons from the passive scattering beam line.

To the best of our knowledge, this is the first study to compare Monte Carlo secondary neutron dose estimates in clinical treatments between these various proton therapy modalities and to realistically quantify the secondary neutron dose contribution of clinical pMBRT treatments. The method established in this study will enable epidemiological studies of the long-term effects of intracranial treatments at ICPO, notably radiation-induced second malignancies.

1. Introduction

More than half of patients with cancer undergo radiation therapy (RT) **(Delaney *et al* 2005, Baskar *et al* 2012)**, with proton therapy (PT) emerging as an advanced form of RT for the treatment of cancer. The key advantage of this modality is the ability to achieve a more conformal coverage of the target volume, while reducing the **integral** dose delivered compared to photon radiation therapy (Lomax *et al* 1999). However, unlike x-rays that require a minimum energy of around 10 MeV to produce a significant quantity of neutrons and mostly in the treatment head (Zanini *et al* 2004), production of secondary neutrons is inevitable in proton therapy and is not taken into account during treatment planning. In active scanning proton therapy, in which pencil beams are magnetically deflected to scan the tumor region, neutrons are mainly produced inside the patient while for passive scattering the majority of neutrons are produced by the scattering elements of the nozzle, the range modulator wheel, as well as beam shaping devices such as brass collimators and compensators. In addition, neutrons deposit the dose throughout the body and while their radiobiological effect is not well known, it is thought to be much larger than that of photons (Hälg and Schneider 2020).

The Institut Curie Orsay Proton Therapy Center has a long history of proton therapy for the treatment of cancer that started with a fixed passive scattering beam line. For example, since 1993, 1,038 pediatric patients have been treated by passive scattering and 144 have been treated by active scanning. In order to study the contribution of neutrons to organs at risk, experimental measurements (Farah *et al* 2014, 2015, Bonfrate *et al* 2016a, De Marzi *et al* 2019) and Monte Carlo simulations (Sayah *et al* 2013, 2014, Bonfrate *et al* 2016b) have been extensively used to assess exposure of healthy organs to stray neutrons with these two beam delivery modes at our institution. Many patients undergoing cancer treatment can now expect a long-term survival prognosis. Since second malignancies and toxicities take time to occur, they can have a greater impact on the patient's quality of life, particularly in pediatric patients who represent a larger proportion of patients treated by proton therapy and who have a longer life expectancy, but at the same time are at greatest risk of developing radiation-induced second malignancies due, among other things, to their smaller size and their more radiosensitive tissues (Council 2006).

The secondary neutron dose received by a patient receiving proton therapy has been shown (Bonfrate *et al* 2016b, Sayah *et al* 2014, Zacharatou Jarlskog *et al* 2008) to be highly dependent on age and size, as well as tumor morphology and location in addition to the beam line configuration and field parameters such as the range, spread out Bragg peak width and angular incidence. Given the complexity and treatment specificity of the neutron dose distribution, the purpose of this work was twofold: to develop and validate methods to accurately estimate the dose delivered to normal tissues of pediatric or adult proton therapy patients; to develop computational tools to perform a comprehensive comparison of normal tissue dose and risk across different proton beams, laying ground for epidemiological investigations to correlate the radiobiological effects of stray neutrons with second cancers.

Pencil beam scanning and double scattering techniques were both considered in this study, as well as a more recent spatial dose fractionation technique - proton minibeam radiation therapy (pMBRT). pMBRT is an innovative form of radiotherapy actively studied at Institut Curie, in which submillimeter pencil beams separated by a few millimeters modulate the spatial dose distribution, resulting in a homogeneous dose distribution in the tumor region, with a peak and valley distribution in the transverse profile of healthy tissues. This

technique has shown promising results, notably in the preservation of healthy tissues while achieving tumor control (Prezado *et al* 2017, Lamirault *et al* 2020a, 2020b), allowing dose escalation in radioresistant tumors, such as high-grade glioma. However, at the present time, minibeams are produced using the PBS technique in tandem with a brass collimator with linear slits, which is expected to increase the neutron yield. It is therefore important to estimate the neutron dose of this new irradiation modality, and compare it with those of more conventional techniques.

2. Methods

The Proton Therapy Center of Institut Curie houses an IBA universal nozzle supplied by a 230 MeV Proteus IBA proton cyclotron and is capable of delivering both PBS and DS treatment modalities. A realistic estimation of the secondary absorbed neutron dose in a patient undergoing treatment can only be made by using Monte Carlo algorithms that incorporate the physics at play, **as well as the detailed geometry and respective materials of the treatment room including the gantry concrete walls and the universal nozzle based on the technical drawings provided by IBA, in addition to the patient**. The Geant4 framework TOPAS v3.5 (Perl *et al* 2012) based on Geant4.10.06.p1 was used to model the ICPO nozzle, which has been thoroughly validated in both DS (Bonfrate *et al* 2016a) and PBS (De Marzi *et al* 2019), as well as pMBRT (De Marzi *et al* 2018, Lansonneur *et al* 2020) by comparing simulated and measured dose distributions in water, as well as extensive comparisons with our treatment planning systems. The physics list includes the following physics libraries: "g4em-standard_opt3", "g4h-phy_QGSP_BIC_HP", "g4decay", "g4ion-binarycascade", "g4h-elastic_HP", "g4stopping" and "g4radioactivedecay". The first part of this work describes the benchmarking of MC neutron simulations against measurements, while the second part evaluates the secondary neutron dose received by three patients representative of intracranial treatments conducted at ICPO, as well as a comparison of the three irradiation techniques. To our knowledge, this is the first comprehensive study to compare Monte Carlo secondary neutron dose estimates in clinical treatments between these various proton therapy modalities.

2.1 Assessing the neutron ambient dose equivalent in the treatment room

In order to validate the Monte Carlo model of the secondary neutron dose in the ICPO gantry room, we carried out a campaign of measurements to benchmark the simulations. The **extended-range Wide** Energy Neutron Detection Instrument (WENDI-II) counter (Olsher *et al* 2000) was used to measure the neutron ambient dose equivalent, H*(10), at different locations of the treatment room. The wide energy neutron detector is an Anderson-Braun type rem counter that measures the ambient dose equivalent deposited by neutrons inside the active volume of the detector. This detector is especially suited to this work as it covers an energy range from thermal to 5 GeV neutrons. Indeed, H*(10) is a commonly used ambient dose equivalent quantity to conservatively estimate the protection quantities. H*(10) is defined as the dose equivalent that would be produced by the corresponding expanded and aligned field in the International Commission on Radiation Units and Measurements (ICRU) sphere (15 cm radius) at a depth of 10 mm on the radius opposing the direction of the aligned field (ICRP 1996) and is defined as

$$H^*(10) = \sum_{i=1}^{n} h^*(10)_i \times \emptyset_i \,, \quad (1)$$

where $\emptyset_i$ is the neutron fluence for energy bin i and $h^*(10)_i = H^*(10)/\emptyset_i$ is the fluence-to dose-equivalent conversion coefficient for energy bin i. The values of $h^*(10)_i$ for various

neutron energies were taken from ICRP Publication 74 (ICRP 1996). **The response of the WENDI-II detector was determined experimentally by irradiating it with nine monoenergetic neutron beams of energy between 144 keV and 17 MeV delivered by the AMANDE installation (IRSN, France). Regarding the fluence and dose equivalent reference, the neutron fluence energy distributions were measured by two types of recoil proton spectrometers as a function of neutron energy.**

Measurements were carried out with the gantry at 270° and at four different positions: A, B, C and D with respect to a 34×40×35 cm^3 water phantom positioned downstream of the beam line with its surface at isocenter; and **monoenergetic** proton beams with different energies: 100 MeV, 150 MeV and 200 MeV. **DS and pMBRT irradiations were performed**

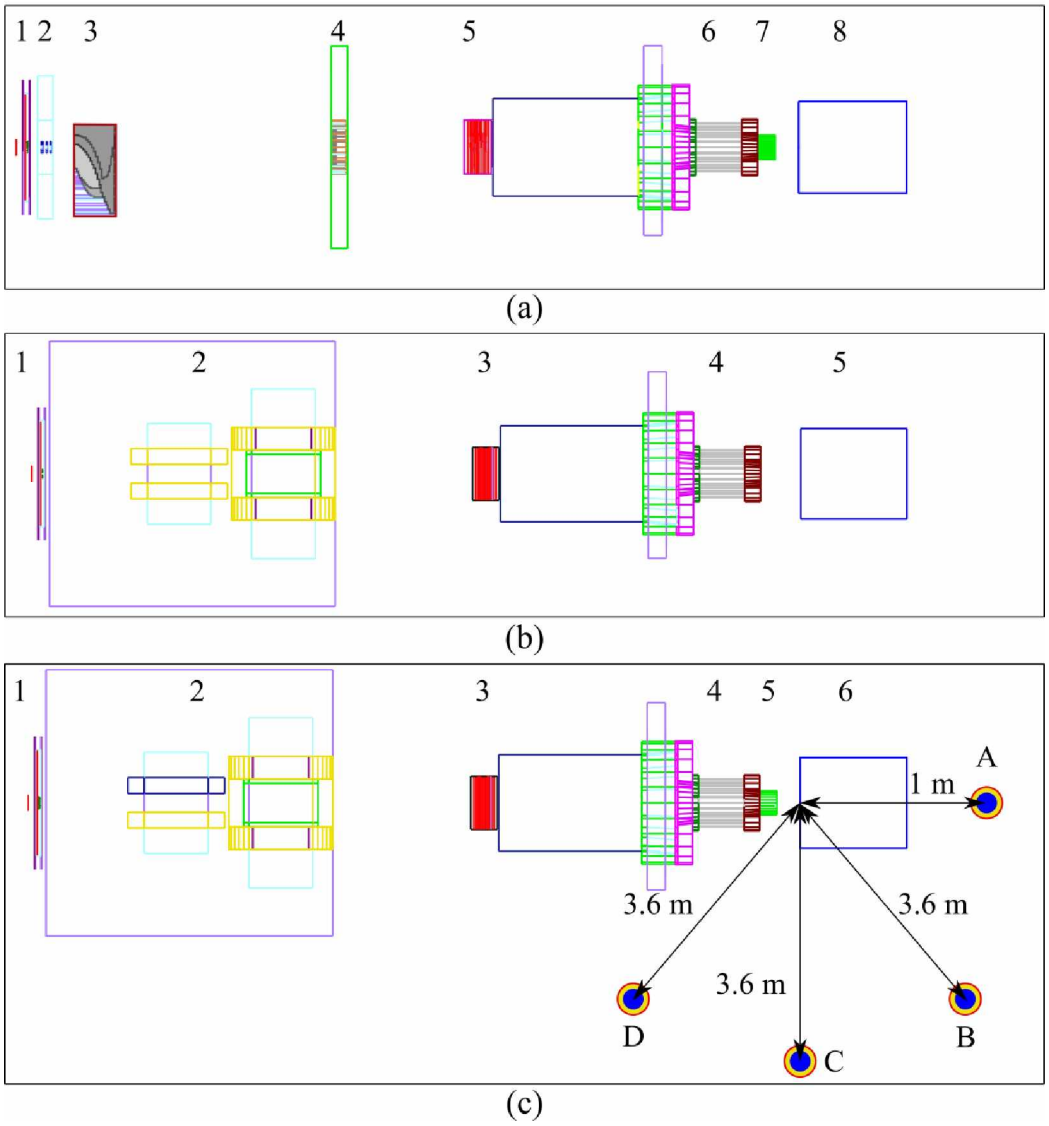

Figure 1. Topas model of the IBA Universal Nozzle and water tank positioned with the surface at isocenter. The double scattering nozzle (a) contains monitoring ionization chambers (1,5), a combination of tantalum scatterers (2), a range modulator wheel (3), a second tantalum and lead scatterer (4), **a snout (6)** and a brass collimator and compensator (7). The PBS nozzle (b) also used for pMBRT (c) includes monitoring ionization chambers (1,3) as well as the scanning magnets (2), a snout **(4)** and a vertical slit collimator in the case of pMBRT (5). The position of the WENDI-II counter is shown in (c) as concentric circles: the counter was positioned 1 m away from water tank suface on the same axis as the nozzle - position A, and 3.6 m further away at positions B, C and D from the axis.

with a 65 mm thick brass collimator. In DS the collimator had a circular aperture of 5.5 cm diameter, while the collimator in pMBRT had five 0.4 mm wide slits separated by a center-to-center distance of 4 mm. The feasibility of the pMBRT collimator configuration was previously validated experimentally by De Marzi *et al* (2018) and was used by Lansonneur *et al* (2020) in the calculation of pMBRT treatment plans showing a good compromise between dose homogeneity in the target region and spatial fractionation of the dose in healthy tissues. The geometry of the experimental setup is illustrated in Figure 1 including the universal nozzle configuration for PBS, DS and pMBRT. A scanned field size of 5×5 cm^2 was used for PBS and pMBRT irradiation. All measurements of H*(10), with the exception of pMBRT, were normalized to the proton absorbed dose in water (Gy), measured with an IBA PPC05 ionization chamber at the entrance of the water phantom**, corresponding to the entrance plateau of the Bragg peak**. **This position allows for a much better precision of the comparison of the measured dose with that of MC-calculated, since at the entrance of the plateau the dose gradient is very small (longitudinally and transversally) and also avoids uncertainties due to the difficult positioning the ionization chamber in the Bragg peak, where the dose gradients are much larger.** The pMBRT neutron ambient dose was normalized in the same way as for PBS but taking into account the fraction of protons that are able to pass through the multi-slit collimator. The total relative uncertainty of the measurements was estimated to be of the order of 22%.

The Monte Carlo simulation comprises the ICPO IBA Universal Nozzle with both PBS and DS modalities, **as well** as the room geometry including the concrete walls, which are important **to** the estimation of thermal neutrons, and the water phantom. **We have estimated that in the presence of the gantry concrete walls H*(10) is about 20% larger than if the walls were not considered in the modelling of PBS. Sayah (2012) simulated the ambient neutron dose equivalent in the same DS gantry and reported that in the presence of walls, H*(10) increases from 21% to 46% and that the epithermal (< 10keV) component of the neutron spectrum is mainly due to scattered neutrons in the room, leading to a shift of the mean energy from 2 MeV to 4 MeV when including the walls, to 6 MeV to 18 MeV in their absence.** The TOPAS' "Ambient Dose Equivalent" scorer for neutron particles was applied to tally the neutron ambient dose equivalent. TOPAS evaluates the neutron fluence as a function of the energy spectrum and then multiplies it by fluence-to-dose equivalent conversion to obtain the ambient dose equivalent as in equation (1). A maximum relative statistical uncertainty of 6% on the calculated H*(10) values was obtained by simulating about 10^8 protons. **In addition to simulations performed with the binary cascade model used in "g4h-phy_QGSP_BIC_HP" (Wellisch *et al* 2005), we have also done simulations using the "g4h-phy_QGSP_BERT_HP" physics library, which applies the Bertini model (Wright and Kelsey 2015) in the calculation of intra-nuclear cascades, as we have found to be in better agreement with the measurements.**

2.2 Secondary neutron dose in intracranial treatments

Three clinically relevant intracranial treatment plans for patients of different age groups and different statures, herein referred to as **P1A (pediatric patient, 12 months of age), P7A (pediatric patient, 7 years of age)** and adult patients, were chosen to investigate the secondary neutron dose contribution due to each irradiation technique. As demonstrated by the work of Zacharatou Jarlskog *et al* (2008) and Bonfrate *et al* (2016b), the neutron dose is highly dependent on the patient's position and distance relative to the nozzle, as well as

Table 1. Treatment **plan** summary for the three patients considered for pencil beam scanning, proton minibeam radiation therapy and double scattering irradiation.

	P1A, AT/RT			P7A, Ewing sarcoma			Adult, Clival chordoma		
PBS, pMBRT	Beam 1	Beam 2	Beam 3	Beam 1	Beam 2	Beam 3	Beam 1	Beam 2	Beam 3
Energy (MeV)	113.2-161.3	103.9-149.5	121.6-163.9	132.5-169.4	102.9-141	104.4-150	130.5-178.9	117.3-166.4	128.7-172.7
Modulation width (cm)	9.7	8.46	9	8.29	8.89	8.73	9.94	10.72	9.63
Gantry angle	305°	105°	270°	270°	160°	225°	300°	140°	220°
Prescribed dose Gy(RBE)	18.36	18.36	17.28	16.2	21.6	16.2	19.8	19.8	19.8
Monitor units: PBS, pMBRT	121.6, 2108.3	235.7, 1997.4	101.45, 1692.5	76.8, 1313.8	123.05, 1782.6	94.0, 1754.8	97.0, 1564.4	100.9, 2450.5	113.5, 2555.1
DS	Beam 1	Beam 2	Beam 3	Beam 1	Beam 2	Beam 3	Beam 1	Beam 2	Beam 3
Energy (MeV)	169.4	183.2	173.6	179.5	169.3	181.9	189.5	176.5	182.4
Modulation width (cm)	9.7	8.46	9.06	8.29	8.89	8.73	7.42	6.55	5.31
Gantry angle	305°	105°	270°	270°	160°	225°	300°	140°	220°
Prescribed dose Gy(RBE)	18.36	18.36	17.28	16.2	21.6	16.2	19.8	19.8	19.8
Monitor units	1557.8	1409.4	1501.1	1374.5	1832.7	1276.4	1640.0	1640.0	1500.0

beam parameters. We therefore simulated the same treatment plan for each irradiation modality, i.e. the same prescribed doses and field angles, and adapted it appropriately. The Eclipse v15.5 (Varian Medical Systems, Palo Alto, USA) treatment planning system was used to optimize the PBS treatment plan using the intensity-modulated proton therapy (IMPT) technique, while ISOgray (DOSIsoft, Cachan, France) was used for DS. As the patients were originally treated at ICPO with PBS, the DS treatment plan was therefore optimized on the basis of **the** already established PBS treatment plan. **The pMBRT treatment plan was identical to the PBS treatment plan, as in our pMBRT approach the pencil beam scanning delivery mode is combined with a multi-slit collimator**. However, a larger number of protons is needed to deliver the prescribed dose to the planning target volume (PTV), given that the multi-slit collimator reduces the number of particles that reach the patient. The methodology used to generate the pMBRT plan is based on that described by Lansonneur *et al* (2020), in which the center-to-center distance of the slits and the slit size were optimized for each field and each patient to conserve dose homogeneity in the PTV, while a peak-and-valley dose distribution is observed in healthy tissues. A summary of the treatment plans can be found in table 1. All procedures involving patient data (fully anonymized) were in accordance with the ethical standards, guidelines and regulations of the Institut Curie ethics committee and with the 1964 Helsinki declaration and its later amendments or comparable ethical standards (approval number DATA200003). Since gathered patient data was retrospective and did not directly involve the human participants during this theoretical work, informed consent was also not applicable to this study.

Intracranial treatments are based on the patients' partial body CTs to optimize the proton dose distribution. However, calculation of the secondary neutron dose to the patient's

Table 2. Information of patients and matched phantoms used in this study. The naming convention for the UF phantom series according to Geyer *et al* (2014) begins with the identifier UFH (University of Florida Hybrid),followed by the reference phantom age in years (01, 05, AD for adult) and then the phantom gender (M for male and F for female).

	Age	Genter	Height (cm)	Weight (kg)
P1A				
Patient	10 months	M	68	8.1
Phantom UFH01M	1 year	M	85	10
P7A				
Patient	7 years	M	111	17
Phantom UFH05M	5 years	M	115	20
ADULT				
Patient	54 years	F	165	50
Phantom UFHADF	30 years	F	165	50

body requires a whole body CT image, as normal tissues of interest may be located outside the CT coverage. As also described by Kuzmin *et al* (2018), to extend the partial patient anatomy to the whole body, the head CT scan of each patient was merged with a computational phantom in DICOM format with corresponding age, size and gender, **summarized in table 2**, developed by the University of Florida (UF) and the US National Cancer Institute (US-NCI) (Lee *et al* 2010)**.** These phantoms belong to the UFH family of hybrid phantoms of different ages, sizes and both genders and represent the ICRP reference phantoms including the reference organ masses from ICRP Publication 89 (ICRP 2002), the reference tissue densities and elemental compositions from both ICRP Publication 89 and Report 46 by the International Commission on Radiation Units and Measurements (1992).
The merging procedure was performed using LifEx freeware (Nioche *et al* 2018) and resulted in a whole body image, in which the upper part was composed of the patient's CT and the lower part of the phantom's CT.

A python script developed at ICPO converted the treatment plans into TOPAS parameter files that were then used to realistically simulate **the** treatment, including the prescribed range and modulation of each beam, which were then converted into the corresponding scatterers and range modulator wheel, as well as beam-specific collimators and compensators in DS and the spatial and intensity distribution of the spots in PBS. The proton and neutron doses were scored in a $2\times2\times2$ mm^3 dose grid, using the TOPAS "DoseToWater" scorer with the "OnlyIncludeParticleOrAncestorNamed" **filter** to tally the neutron dose. The dose distribution in patients was simulated for each treatment beam, using 10^8 - 10^9 particles corresponding to a relative statistical uncertainty of less than 1%. **Organ-specific neutron doses were then evaluated for in-field organs, here defined here as the organs located in the patients' head and comprising the brainstem, the right and left temporal lobe, the chiasma, the brain, the left and right optic nerves, and the eyes; and for out-of-field organs here defined as organs located outside of the patients' head including the thyroid, the bone marrow, the heart, the spleen, the stomach, the liver, the pancreas, the kidneys, the colon, the small bowel, the testes, the scrotum, the bladder, the penis, the prostate, the ovaries and the uterus.**

3. Results

3.1 Benchmarking the neutron ambient dose equivalent in the treatment room

Neutron ambient dose equivalent values were measured with the WENDI-II detector for four positions in the gantry room and three proton beam energies. A summary of the results is presented in table **3** together with the corresponding MC calculations and their percentage differences. **The uncertainties on the measured values correspond to the estimated relative uncertainty of 22%, which takes into account the relative uncertainty on the angular response and the uncertainty on the correction factor of the energy response of the instrument, while the uncertainties on the MC neutron ambient dose values account for relative statistical uncertainties. All reported uncertainties are 1 standard deviation statistical uncertainties.**

Figure **2** shows a comparison of the H*(10)/Gy values with those of Monte Carlo calculations for PBS, DS and pMBRT irradiations, for the various positions and proton beam energies. As expected, MC-calculated H*(10) in PBS decreases with increasing angle with respect to the beam axis, and it increases with increasing proton energy from 7.63±0.09 $\mu Sv.Gy^{-1}$ at 100MeV to 135.6±0.4 $\mu Sv.Gy^{-1}$ at 200MeV at position A as more energetic protons produce more neutrons. PBS irradiation produces a very small quantity of neutrons, while, with double scattering, the dose increases by a factor of 5 to 1213. The brass collimator in pMBRT results in an increase of 5 to 75 of the neutron ambient dose when compared to PBS, which is still lower than that of DS.

Monte Carlo simulations**, using the Binary cascade model**, and neutron ambient dose measurements had a minimum and maximum relative difference of 17% (100 MeV, D) and 269% (150 MeV, A), respectively, for PBS, 3% (150 MeV, D) and 117% (100 MeV, A), respectively, for pMBRT, and **60% (150 MeV, D)** and 233% (100 MeV, B), respectively, for DS. **With the Bertini model the minimum and maximum relative difference for PBS was of 5% (100 MeV, C) and 75% (200 MeV, B), respectively, 3% (100 MeV,D) and 87% (100 MeV, A), respectively, for pMBRT, and 27% (100 MeV, A) and 194% (100 MeV, B), respectively, for DS.** Other published studies have reported similar discrepancies: Charyyev and Wang (2020) investigated the neutron ambient dose equivalent in spatially fractionated radiotherapy and reported a 9% to 123% **relative** difference between MC simulations and measurements, while Farah *et al* (2014), **who used the Bertini intra-nuclear cascade model,** obtained a difference ranging from 6% to 138% between double scattering measurements and MC simulations.

3.2 Evaluation of the secondary neutron dose in intracranial treatment

The secondary neutron dose per prescribed biological dose for selected organs of the **P1A, P7A** and adult patients, and for the three irradiation modalities considered is shown in **Figure 4**. **The physics list "g4h-phy_QGSP_BIC_HP" that employs the binary cascade model was used in the calculations of the secondary neutron dose since the goal was to compare the organ-specific secondary neutron dose of the three irradiation techniques.** A general tendency was observed irrespective of the irradiation technique in which the neutron dose decreases with increasing distance of the organs with respect to the irradiated target area. Across all irradiation techniques, pMBRT consistently resulted in greater neutron production in the in-field organs, due to the presence of the vertical slit collimator that reduces the number of protons that are able to reach the patient (fewer than 10%). This

Table 3. Measured (M) and Monte Carlo simulated (MC) neutron ambient dose equivalent normalized to the proton dose at the entrance plateau of the Bragg peak in $\mu Sv.Gy^{-1}$ units, for different positions and different proton beam energies for pencil beam scanning, proton minibeam radiation therapy and double scattering irradiations, as well as their relative percentage differences: Diff (%)=(M-MC)/M×100. **The MC values include those calculated with the "g4h-phy_QGSP_BIC_HP" physics library (top values) and those calculated with the "g4h-phy_QGSP_BERT_HP" physics library (bottom values).**

	PBS			pMBRT			DS		
				A					
Energy (MeV)	M	MC	Diff (%)	M	MC	Diff (%)	M	MC	Diff (%)
100	2.2±0.5	7.63±0.09 3.67±0.05	247 67	23±5	51±1 43±0.9	117 87	146±33	239±7 185±6	64 27
150	12±3	44.3±0.2 19.1±0.1	269 59	125±28	243±3 174±2	94 39	182±49	483±9 351±8	165 93
200	-	135.6±0.4 57.8±0.2	-	304±68	627±6 444±4	106 46	205±46	655±8 443±6	219 116
				B					
Energy (MeV)	M	MC	Diff (%)	M	MC	Diff (%)	M	MC	Diff (%)
100	0.23±0.05	0.51±0.02 0.28±0.01	122 22	23±5	45±1 42.4±0.9	96 84	112 ± 25	373±9 329 ±9	233 194
150	0.7±0.2	1.63±0.04 1.04±0.03	133 49	57±13	111±2 100±1	95 75	167±37	492±10 458±9	195 174
200	1.3±0.3	3.68±0.07 2.28±0.05	183 75	101±23	208±2 186±2	106 84	145±32	390±6 356±6	169 145
				C					
Energy (MeV)	M	MC	Diff (%)	M	MC	Diff (%)	M	MC	Diff (%)
100	0.21±0.06	0.27±0.02 0.20±0.01	29 5	28±6	43±1 41.8±0.9	54 49	131±29	359 ±9 337 ± 9	174 157
150	0.6±0.1	0.89±0.03 0.63±0.02	48 5	64±14	109±2 103±1	70 61	182±41	427±9 393±8	135 116
200	1.1±0.2	2.00±0.05 1.35±0.03	45 23	112±25	202±2 186±2	80 66	142±32	310±6 287±5	118 102
				D					
Energy (MeV)	M	MC	Diff (%)	M	MC	Diff (%)	M	MC	Diff (%)
100	0.29±0.06	0.34±0.02 0.32±0.01	17 10	29±7	30.9±0.8 28.1±0.7	6 3	167±37	474±11 431±10	183 138
150	0.6±0.1	0.77±0.03 0.72±0.02	28 20	65±14	67±1 62.6±0.9	3 4	202±45	508±10 476±10	151 136
200	1.0±0.2	1.37±0.04 1.24±0.03	27 24	110±25	118±1 113±1	7 3	147±33	370±6 344±6	152 134

resulted in an increase in the number of protons required to achieve the prescribed dose at the PTV, and subsequently resulted in a greater production of neutrons from the collimator. However, for the out-of-field organs, the neutron dose ratio of DS to pMBRT became increasingly larger as the organ considered was situated further away from the PTV. These neutrons are produced in the multiple beam line elements of the DS nozzle and can reach the patient's body, contributing to the total dose.

Tables A1 to A3 summarize the absorbed neutron dose per prescribed dose for PBS, DS and pMBRT for a few selected organs. A statistical relative uncertainty of less than 1% was obtained for organs close to the PTV, while the relative uncertainty for organs situated further away was less than 3%. The mean neutron dose received by the P1A patient undergoing double scattering irradiation was 1.2-fold higher for in-field organs and 6.2-fold higher for out-of-field organs, compared to the PBS technique. The mean neutron dose delivered by pMBRT was 2.6-fold higher for in-field organs, and 7.2-fold higher for out-of-field organs compared to PBS, and 2.2-fold higher for in-field organs and 1.2-fold higher for out-of-field organs compared to DS. The cumulative dose for out-of-field organs ranged from 0.2 mGy to 8.8 mGy (testes, thyroid) with PBS, from 2.2 mGy to 43.4 mGy (testes, thyroid) for pMBRT and from 6.0 mGy to 14.5 mGy (scrotum, thyroid) for DS. For the P7A patient, the mean neutron dose delivered by DS was 1.5-fold higher for in-field organs and 27.4-fold higher for out-of-field organs compared to PBS. The use of a minibeam collimator increased the in-field neutron dose by a factor of 3.9 and the out-of-field dose by a factor of 11.7 compared to PBS; similarly, the in-field neutron dose with pMBRT was 2.6-fold higher than that delivered by DS, while the beam line elements of DS resulted in a 2.3-fold higher out-of-field dose compared to pMBRT. The cumulative dose for out-of-field organs ranged from 70.2 µGy to 406 µGy (penis, spleen) for PBS, from 0.8 mGy to 4.8 mGy (testes, spleen) for pMBRT and from 3.7 mGy to 7.8 mGy (penis, spleen) for DS. The secondary neutron dose tendencies for the adult patient were very similar to those observed in the P7A patient,

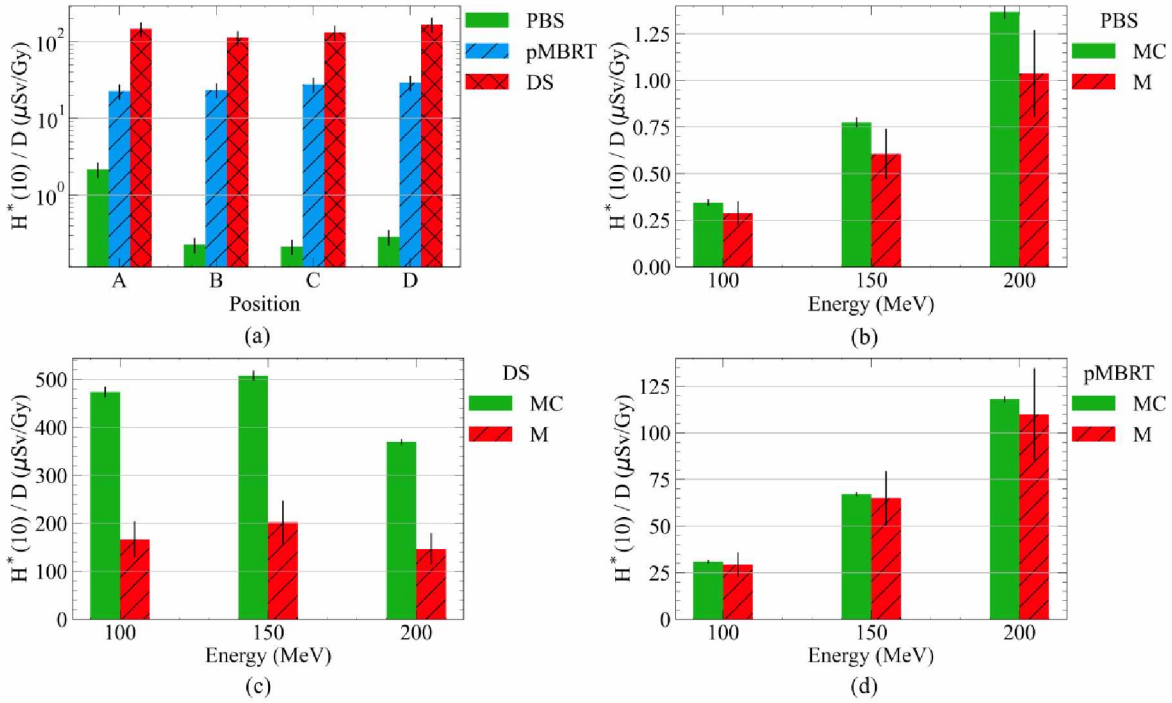

Figure 2. The neutron ambient dose equivalent (H*(10)) per proton dose in the gantry room at the Institut Curie Orsay Proton Therapy Center for different positions and different proton beam energies. (a) Comparison of the measured H*(10) for pencil beam scanning, proton minibeam radiation therapy and double scattering as a function of the measurement position. Comparison of measured and MC simulated H*(10) per proton dose for three different proton beam energies in positon D in pencil beam scanning (b), proton minibeam radiation therapy (c) and double scattering (d). **The "g4h-phy_QGSP_BIC_HP" physics library was used in the Monte Carlo calculations shown in these graphs.**

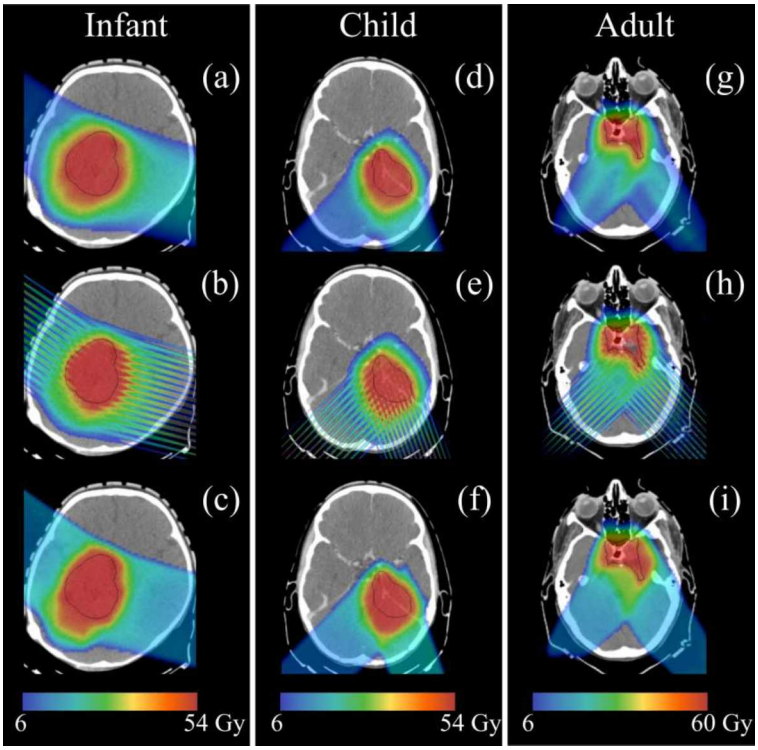

Figure 3. Dose distribution for the P1A, P7A and adult patients. Pencil beam scanning dose distributions are shown in (a), (d) and (g); proton minibeam radiation therapy doses in (b), (e) and (h); and double scattering doses in (c), (f) and (i). The PTV of each patient is outlined in black.

with a cumulative dose for out-of-field organs ranging from 52 µGy to 720 µGy (bladder, heart) for PBS, from 0.9 mGy to 11.4 mGy (uterus, heart) for pMBRT and from 2.9 mGy to 9.0 mGy (bladder, heart) for DS.

4. Discussion

In PBS mode the neutron ambient dose equivalent per proton dose was of the order of a few $\mu Sv.Gy^{-1}$, as in the study by Mojżeszek *et al* (2017), who reported doses of 0.14±0.06 $\mu Sv.Gy^{-1}$ (100 MeV), 0.75±0.30 $\mu Sv.Gy^{-1}$ (150 MeV), 1.84±0.74 $\mu Sv.Gy^{-1}$ (200 MeV), while we measured 0.23±0.05 $\mu Sv.Gy^{-1}$, 0.7±0.2 $\mu Sv.Gy^{-1}$ and 1.3±0.3 $\mu Sv.Gy^{-1}$, respectively, for the same field size and position relative to the beam axis (B), although 2.1m further away from the water phantom. For pMBRT, a maximum dose increase factor of 95 compared to PBS is comparable to that reported by Charyyev and Wang (2020), who measured a 40-fold higher secondary neutron dose when a physical collimator was used to generate minibeams. The measured results for double scattering irradiation were largely concordant with those reported in the literature, with H*(10) per absorbed proton dose of the order of several hundred $\mu Sv.Gy^{-1}$, depending on the distance from the isocenter, angular position and proton beam energy. The results for the DS irradiation were very similar to those reported by Farah *et al* (2014): 155 $\mu Sv.Gy^{-1}$ (B), 255 $\mu Sv.Gy^{-1}$ (C), and 195 $\mu Sv.Gy^{-1}$ (D) for 178 MeV protons measured by a WENDI-II counter, while we measured 146±33 $\mu Sv.Gy^{-1}$, 143±32 $\mu Sv.Gy^{-1}$ and 148±33 $\mu Sv.Gy^{-1}$ for 200MeV, respectively.

Our simulated results for the secondary neutron dose in intracranial treatments clearly demonstrate the advantage of PBS to reduce the of out-of-field secondary neutron dose. For the P1A patient, the ratio between the maximum neutron dose (brainstem) and the minimum

neutron dose (testes) was 302, compared to 8 for DS (brainstem to scrotum) and 46 for pMBRT (brainstem to testes). For the adult patient, in whom the out-of-field organs were situated further away from the nozzle, the dose reduction was even more marked, with a ratio between the maximum dose (brainstem) and the minimum dose (bladder) of 935 for PBS, 25 for DS and 194 for pMBRT. These results indicate that a large proportion of the secondary neutron absorbed by organs with DS and pMBRT is due to external neutrons, resulting in a considerably higher secondary neutron dose even at a great distance from the target treatment volume. For PBS, however, neutrons are mainly produced in the patient's body and the neutron dose, therefore, decreases with distance from the PTV. Interestingly, for out-of-field organs, particularly those situated further away from the PTV, the neutron dose is higher with DS than with pMBRT, although this tendency was not observed for in-field organs, which can be attributed to the fact that DS comprises more beam line elements in addition to the collimator and compensator that are also present in pMBRT.

A previous study of the secondary neutron dose in computational phantoms for passive scattering but modelled with MCNPX, was performed by Sayah *et al* (2014) for the same gantry room, but using a simplified set-up, as the same spherical tumor was modelled for patients of different ages and using identical treatment plans. The ratio between their results and those reported here is about 3:5 for several organs and across age-groups. Sayah *et al* reported a mean neutron dose of 252 μGy.Gy(RBE)$^{-1}$ to the thyroid for a 1-year-old phantom, while we estimated a total dose of 268 μGy.Gy(RBE)$^{-1}$ for three fields for our 1-year-old patient. For the adult patient, Sayah *et al* (2014) reported a dose of 102 μGy.Gy^{-1} to the heart while we reported a dose of 203 μGy.Gy(RBE)$^{-1}$. Our results for PBS are comparable to those reported by Yeom *et al* (2020), who studied the secondary neutron dose for intracranial and craniospinal irradiations of pediatric patients. They reported a neutron dose of 0.05 Gy(RBE).Gy(RBE)$^{-1}$ for the brain and 2.1 μGy(RBE).Gy(RBE)$^{-1}$ for the testes, while we reported doses of 0.57 mGy.Gy(RBE)$^{-1}$ and 3.5 μGy.Gy(RBE)$^{-1}$, respectively, for a patient of identical age.

This work focuses on the comparison of the neutron absorbed dose between three different modes of irradiation. The evaluation of neutron dose equivalent values relies on the knowledge of the RBE for which there is a large uncertainty, in particular the neutron RBE (NCRP 1990) . Furthermore, there are several physical parameters that differ among the three irradiation modes we compared, such as for example the dose rate or fractionation schemes. The biological mechanisms involved in pMBRT are also still largely unknown and seem to differ from those of conventional irradiation; therefore, in this study, we did not extrapolate the current knowledge on the dependence of the neutron RBE, on neutron dose for this technique.

This study presents a number of limitations. Firstly, the models used were derived from a small number of clinical cases and a limited number of field orientations were studied, which has been shown to greatly affect the secondary neutron component. Secondly, merging of the patients' CT scans phantom CT scans did not allow the calculation of the neutron dose in organs situated at the border of each CT. This limitation could be resolved by judiciously choosing the CT merging point to avoid including organs of interest. **In what concerns the uncertainties of the reported simulations, in this work the gantry structure that rotates the isocentric arm and the bending magnets were not modelled and may contribute to the observed differences between measured and MC-calculated H*(10) values, as they can influence the neutron spectra (Farah *et al* 2014). Another source of uncertainty lies in the physics models used in the Monte Carlo calculations, Arce *et al* (2021)**

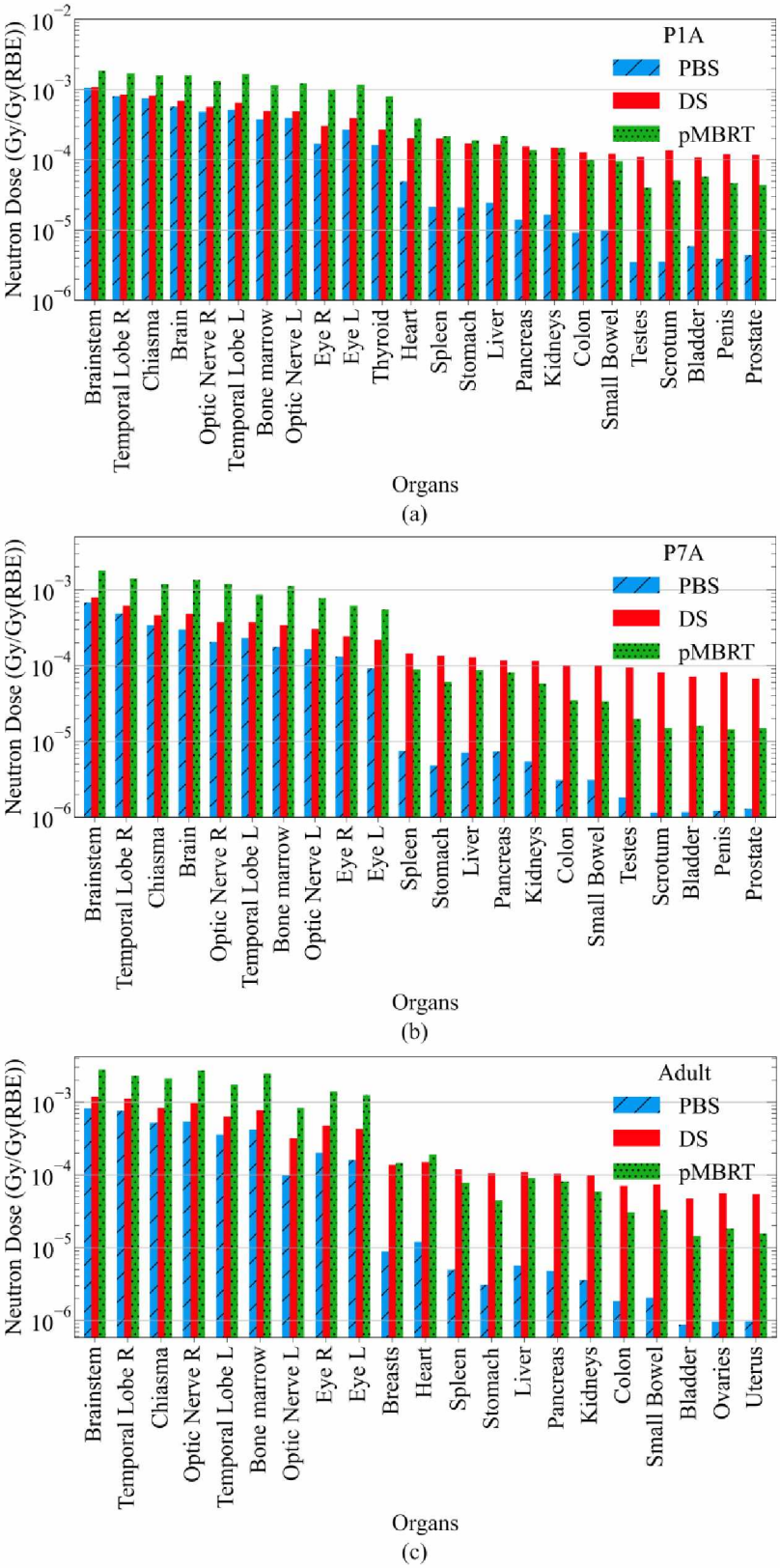

Figure 4. Secondary neutron dose per prescribed RBE dose for selected organs of the P1A (a), P7A (b) and adult (c) patients and for the three irradiation modalities considered: pencil beam scanning, double scattering and proton minibeam radiation therapy. Abbreviations: R – right, L – left.

benchmarked Geant4, in which TOPAS is based, for medical physics applications and reported that in water the neutron yields can be overestimated by up to 50% for protons with energies between 113 MeV and 256 MeV. We compared ambient neutron dose equivalent values calculated with the binary cascade model and the Bertini model, and obtained a better agreement with the latter. While the benchmarking of physics libraries is beyond the scope of this study, we attribute the observed differences between measured and MC-calculated values largely to the described modelling uncertainties.

5. Conclusion

This work describes a method to simulate secondary neutron dose distributions resulting from scattered, scanned and spatially fractionated proton therapy treatments. It allowed investigation of the expected the secondary neutron dose during representative pediatric treatments using a commercially available clinical proton therapy system. We have benchmarked our MC model that estimates the secondary neutron dose by comparing it with measurements obtained using a WENDI-II detector. This is the first study to realistically assess the neutron dose contribution of the brass collimator used in pMBRT for clinical treatment. We observed that pMBRT results in an increased secondary neutron dose relative to DS and PBS which is more pronounced in organs situated closer to the irradiated target, while a higher neutron dose was observed in organs situated further away from the target with DS. This method may open up perspectives for epidemiological studies of the long-term effects of these treatments on the patients irradiated at ICPO, notably radiation-induced malignancies.

Acknowledgements

This work was partly funded by the European Union's Horizon 2020 research and innovation program under grant agreement No. 730983 (INSPIRE). This project also received funding from the European Research Council (ERC) under the European Union's Horizon 2020 research and innovation program (grant agreement No. 817908). This work was granted access to the HPC resources of TGCC under allocation 2021-A0100312448 made by GENCI. We acknowledge PRACE for granting us access to the Joliot Curie-SKL (France) computational cluster under the grant agreement 2020225339.

Appendix A

Table A1. Total absorbed neutron dose per prescribed dose, $Gy.Gy(RBE)^{-1}$, for the P1A patient.

	P1A		
Organs	PBS	pMBRT	DS
Brainstem	1.0555E-03 ± 8E-07	1.861 E-03 ± 6E-06	1.090E-03 ± 4E-06
Temporal Lobe L	8.102E-04 ± 7E-07	1.704 E-03 ± 6E-06	8.44E-04 ± 3E-06
Chiasma	7.595E-04 ± 7E-07	1.598 E-03 ± 5E-06	8.26E-04 ± 3E-06
Brain	5.705E-04 ± 4E-07	1.604 E-03 ± 4E-06	6.95E-04 ± 2E-06
Bone marrow	4.799E-04 ± 5E-07	1.316 E-03 ± 5E-06	5.67E-04 ± 3E-06
Optic nerve L	5.160E-04 ± 5E-07	1.656 E-03 ± 5E-06	6.47E-04 ± 3E-06
Temporal Lobe R	3.795E-04 ± 4E-07	1.154 E-03 ± 5E-06	4.91E-04 ± 3E-06

Optic nerve R	3.921E-04 ± 5E-07	1.217 E-03 ± 4E-06	4.86E-04 ± 2E-06
Eye R	1.690E-04 ± 3E-07	9.86 E-04 ± 4E-06	3.05E-04 ± 2E-06
Eye L	2.670E-04 ± 4E-07	1.174 E-04 ± 5E-06	3.91E-04 ± 2E-06
Thyroid	1.633E-04 ± 3E-07	8.04 E-04 ± 4E-06	2.68E-04 ± 2E-06
Heart	4.93E-05 ± 2E-07	3.85 E-04 ± 2E-06	2.03E-04 ± 2E-06
Spleen	2.12E-05 ± 1E-07	2.16 E-04 ± 2E-06	2.01E-04 ± 1E-06
Stomach	2.09E-05 ± 1E-07	1.90 E-04 ± 2E-06	1.71E-04 ± 2E-06
Liver	2.46E-051E-07	2.18 E-04 ± 2E-06	1.67E-04 ± 1E-06
Pancreas	1.41E-05 ± 9E-08	1.38 E-04 ± 1E-06	1.55E-04 ± 1E-06
Kidneys	1.66E-05 ± 1E-07	1.48 E-04 ± 1E-06	1.48E-04 ± 1E-06
Colon	9.16E-06 ± 7E-08	9.9E-05 ± 1E-06	1.28E-04 ± 4E-06
Small Bowel	9.76E-06 ± 7E-08	9.5E-05 ± 1E-06	1.23E-04 ± 1E-06
Testes	3.50E-06 ± 5E-08	4.0E-05 ± 6E-07	1.10E-04 ± 2E-06
Scrotum	3.55E-06 ± 5E-08	5.1E-05 ± 2E-06	1.36E-04 ± 7E-06
Bladder	5.88E-06 ± 6E-08	5.7E-05 ± 1E-06	1.07E-04 ± 1E-06
Penis	3.94E-06 ± 5E-08	4.6E-05 ± 1E-06	1.21E-04 ± 5E-06
Prostate	4.40E-06 ± 6E-08	4.4E-05 ± 9E-07	1.18E-04 ± 1E-06

Table A2. Total absorbed neutron dose per prescribed dose, $Gy.Gy(RBE)^{-1}$, for the P7A patient.

	P7A		
Organs	PBS	pMBRT	DS
Brainstem	6.827E-04 ± 5E-07	1.790E-03 ± 4E-06	7.99E-04 ± 2E-06
Temporal Lobe L	4.880E-04 ± 4E-07	1.422E-03 ± 3E-06	6.20E-04 ± 2E-06
Chiasma	3.449E-04 ± 4E-07	1.194E-03 ± 3E-06	4.65E-04 ± 2E-06
Brain	3.014E-04 ± 2E-07	1.345E-03 ± 2E-06	4.85E-04 ± 1E-06
Bone marrow	2.056E-04 ± 2E-07	1.195E-03 ± 3E-06	3.73E-04 ± 1E-06
Optic nerve L	2.309E-04 ± 4E-07	8.63E-04 ± 3E-06	3.74E-04 ± 2E-06
Temporal Lobe R	1.770E-04 ± 2E-07	1.126E-03 ± 2E-06	3.45E-04 ± 1E-06
Optic nerve R	1.650E-04 ± 3E-07	7.77E-04 ± 2E-06	3.04E-04 ± 1E-06
Eye R	9.18E-05 ± 2E-07	5.53E-04 ± 2E-06	2.20E-04 ± 1E-06
Eye L	1.310E-04 ± 2E-07	6.20E-04 ± 2E-06	2.45E-04 ± 1E-06
Spleen	7.52E-06 ± 5E-08	8.94E-05 ± 7E-07	1.45E-04 ± 9E-07
Stomach	7.36E-06 ± 2E-07	8.12E-05 ± 2E-06	1.17E-04 ± 3E-06

Liver	7.15E-06 ± 5E-08	8.72E-05 ± 6E-07	1.292E-04 ± 8E-07
Pancreas	5.44E-06 ± 5E-08	5.83E-05 ± 5E-07	1.154E-04 ± 9E-07
Kidneys	4.81E-06 ± 4E-08	6.09E-05 ± 5E-07	1.353 E-04 ± 9E-07
Colon	3.10E-06 ± 3E-08	3.41E-05 ± 4E-07	9.97E-05 ± 8E-07
Small Bowel	3.09E-06 ± 3E-08	3.49E-05 ± 4E-07	9.99E-05 ± 8E-07
Testes	1.22E-06 ± 2E-08	1.46E-05 ± 3E-07	8.16E-05 ± 1E-06
Scrotum	1.17E-06 ± 2E-08	1.60E-05 ± 3E-07	7.17E-05 ± 9E-07
Bladder	1.83E-06 ± 3E-08	1.98E-05 ± 3E-07	9.45E-05 ± 8E-07
Penis	1.30E-06 ± 4E-08	1.50E-05 ± 3E-07	6.78E-05 ± 1E-06
Prostate	1.16E-06 ± 2E-08	1.50E-05 ± 2E-07	8.11E-05 ± 7E-07

Table A3. Total absorbed neutron dose per prescribed dose, Gy.Gy(RBE)$^{-1}$, for the adult patient.

Adult			
Organs	PBS	pMBRT	DS
Brainstem	8.15E-04 ± 1E-06	2.797E-03 ± 9E-06	1.182E-03 ± 3E-06
Temporal Lobe L	5.403E-04 ± 7E-07	2.727E-03 ± 8E-06	9.66E-04 ± 2E-06
Chiasma	7.572E-04 ± 8E-07	2.293E-03 ± 7E-06	1.116E-03 ± 3E-06
Bone marrow	9.840E-05 ± 2E-07	8.36E-04 ± 4E-06	3.18E-04 ± 1E-06
Optic nerve L	5.22E-04 ± 1E-06	2.10E-03 ± 1E-05	8.31E-04 ± 3E-06
Temporal Lobe R	4.155E-04 ± 6E-07	2.462E-03 ± 7E-06	7.72E-04 ± 2E-06
Optic nerve R	3.571E-04 ± 6E-07	1.741E-03 ± 7E-06	6.36E-04 ± 2E-06
Eye R	1.589E-04 ± 5E-07	1.252E-03 ± 6E-06	4.28E-04 ±2E-06
Eye L	2.011E-04 ± 6E-07	1.404E-03 ± 6E-06	4.78E-04 ± 2E-06
Breasts	8.9E-06 ± 2E-07	1.47E-04 ± 3E-06	1.372E-04 ± 9E-07
Heart	1.20E-05 ± 2E-07	1.91E-04 ± 3E-06	1.493E-04 ± 9E-07
Spleen	4.98E-06 ± 7E-08	7.7E-05 ± 1E-06	1.181E-04 ± 8E-07
Stomach	4.8E-06 ± 2E-07	8.2E-05 ± 2E-06	1.04E-04 ± 3E-06
Liver	5.71E-06 ± 7E-08	9.0E-05 ± 1E-06	1.098E-04 ± 7E-07
Pancreas	3.59E-06 ± 6E-08	5.9E-05 ± 1E-06	9.81E-05 ± 7E-07
Kidneys	3.08E-06 ± 5E-08	4.48E-05 ± 8E-07	1.051E-04 ± 7E-07
Colon	1.84E-06 ± 3E-08	3.06E-05 ± 6E-07	7.05E-05 ± 6E-07
Small Bowel	2.06E-06 ± 4E-08	3.32E-05 ± 7E-07	7.39E-05 ± 7E-07
Bladder	8.7E-07 ± 2E-08	1.44E-05 ± 4E-07	4.75E-05 ± 5E-07

Ovaries	9.6E-07 ± 3E-08	1.83E-05 ± 5E-07	5.62E-05 ± 6E-07
Uterus	9.7E-07 ±2E-08	1.57E-05 ±4E-07	5.42E-05 ± 5E-07

References

Anon 1996 Conversion Coefficients for use in Radiological Protection against External Radiation **74. Ann. I** (3-4)

Arce P, Bolst D, Bordage M C, Brown J M C, Cirrone P, Cortés-Giraldo M A, Cutajar D, Cuttone G, Desorgher L, Dondero P, Dotti A, Faddegon B, Fedon C, Guatelli S, Incerti S, Ivanchenko V, Konstantinov D, Kyriakou I, Latyshev G, Le A, Mancini-Terracciano C, Maire M, Mantero A, Novak M, Omachi C, Pandola L, Perales A, Perrot Y, Petringa G, Quesada J M, Ramos-Méndez J, Romano F, Rosenfeld A B, Sarmiento L G, Sakata D, Sasaki T, Sechopoulos I, Simpson E C, Toshito T and Wright D H 2021 Report on G4-Med, a Geant4 benchmarking system for medical physics applications developed by the Geant4 Medical Simulation Benchmarking Group *Med. Phys.* **48** 19–56

Baskar R, Lee K A, Yeo R and Yeoh K W 2012 Cancer and radiation therapy: Current advances and future directions *Int. J. Med. Sci.* **9** 193–9

Bonfrate A, Farah J, De Marzi L, Delacroix S, Constant E, Hérault J and Clairand I 2016a Benchmarking Monte Carlo simulations against experimental data in clinically relevant passive scattering proton therapy beamline configurations *Radioprotection* **51** 113–22

Bonfrate A, Farah J, De Marzi L, Delacroix S, Hérault J, Sayah R, Lee C, Bolch W E and Clairand I 2016b Influence of beam incidence and irradiation parameters on stray neutron doses to healthy organs of pediatric patients treated for an intracranial tumor with passive scattering proton therapy *Phys. Medica* **32** 590–9

Charyyev S and Wang C-K K C 2020 Assessment of ambient neutron dose equivalent in spatially fractionated radiotherapy with protons using physical collimators *Radiat. Prot. Dosimetry* **189** 190–7

Council N R 2006 *Health risks from exposure to low levels of ionizing radiation: BEIR VII Phase 2* (National Academies Press)

Delaney G, Jacob S, Featherstone C and Barton M 2005 The role of radiotherapy in cancer treatment: Estimating optimal utilization from a review of evidence-based clinical guidelines *Cancer* **104** 1129–37

Farah J, Bonfrate A, De Marzi L, De Oliveira A, Delacroix S, Martinetti F, Trompier F and Clairand I 2015 Configuration and validation of an analytical model predicting secondary neutron radiation in proton therapy using Monte Carlo simulations and experimental measurements *Phys. Medica* **31** 248–56

Farah J, Martinetti F, Sayah R, Lacoste V, Donadille L, Trompier F, Nauraye C, Marzi L De, Vabre I, Delacroix S, Hérault J and Clairand I 2014 Monte Carlo modeling of proton therapy installations: A global experimental method to validate secondary neutron dose calculations *Phys. Med. Biol.* **59** 2747–65

Geyer A M, O'Reilly S, Lee C, Long D J and Bolch W E 2014 The UF/NCI family of hybrid computational phantoms representing the current US population of male and female

children, adolescents, and adults—application to CT dosimetry *Phys. Med. Biol.* **59** 5225–42

Hälg R A and Schneider U 2020 Neutron dose and its measurement in proton therapy—current State of Knowledge *Br. J. Radiol.* **93** 20190412

Kuzmin G A, Mille M M, Jung J W, Lee C, Pelletier C, Akabani G and Lee C 2018 A Novel Method to Extend a Partial-Body CT for the Reconstruction of Dose to Organs beyond the Scan Range *Radiat. Res.* **189** 618–26

Lamirault C, Brisebard E, Patriarca A, Juchaux M, Crepin D, Labiod D, Pouzoulet F, Sebrie C, Jourdain L, Le Dudal M, Hardy D, de Marzi L, Dendale R, Jouvion G and Prezado Y 2020a Spatially Modulated Proton Minibeams Results in the Same Increase of Lifespan as a Uniform Target Dose Coverage in F98-Glioma-Bearing Rats. *Radiat. Res.*

Lamirault C, Doyère V, Juchaux M, Pouzoulet F, Labiod D, Dendale R, Patriarca A, Nauraye C, Le Dudal M, Jouvion G, Hardy D, Massioui N El and Prezado Y 2020b Short and long-term evaluation of the impact of proton minibeam radiation therapy on motor, emotional and cognitive functions *Sci. Rep.* **10** 13511

Lansonneur P, Mammar H, Nauraye C, Patriarca A, Hierso E, Dendale R, Prezado Y and De Marzi L 2020 First proton minibeam radiation therapy treatment plan evaluation *Sci. Rep.* **10** 1–8

Lee C, Lodwick D, Hurtado J, Pafundi D, Williams J L and Bolch W E 2010 The UF family of reference hybrid phantoms for computational radiation dosimetry *Phys. Med. Biol.* **55** 339–63

Lomax A J, Bortfeld T, Goitein G, Debus J, Dykstra C, Tercier P A, Coucke P A and Mirimanoff R O 1999 A treatment planning inter-comparison of proton and intensity modulated photon radiotherapy *Radiother. Oncol.* **51** 257–71

De Marzi L, Da Fonseca A, Moignier C, Patriarca A, Goudjil F, Mazal A, Buvat I and Hérault J 2019 Experimental characterisation of a proton kernel model for pencil beam scanning techniques *Phys. Medica* **64** 195–203

De Marzi L, Patriarca A, Nauraye C, Hierso E, Dendale R, Guardiola C and Prezado Y 2018 Implementation of planar proton minibeam radiation therapy using a pencil beam scanning system: A proof of concept study *Med. Phys.* **45** 5305–16

Mojżeszek N, Farah J, Kłodowska M, Ploc O, Stolarczyk L, Waligórski M P R and Olko P 2017 Measurement of stray neutron doses inside the treatment room from a proton pencil beam scanning system *Phys. Medica* **34** 80–4

NCRP 1990 *The relative biological effectiveness of radiations of different quality : recommendations of the National Council on Radiation Protection and Measurements* (Bethesda, MD : The Council,)

Nioche C, Orlhac F, Boughdad S, Reuze S, Goya-Outi J, Robert C, Pellot-Barakat C, Soussan M, Frouin F erique and Buvat I 2018 Lifex: A freeware for radiomic feature calculation in multimodality imaging to accelerate advances in the characterization of tumor heterogeneity *Cancer Res.* **78** 4786–9

Olsher R H, Hsu H H, Beverding A, Kleck J H, Casson W H, Vasilik D G and Devine R T 2000 WENDI: an improved neutron rem meter. *Health Phys.* **79** 170–81

Perl J, Shin J, Schumann J, Faddegon B and Paganetti H 2012 TOPAS: An innovative proton Monte Carlo platform for research and clinical applications *Med. Phys.* **39** 6818

Prezado Y, Jouvion G, Hardy D, Patriarca A, Nauraye C, Bergs J, González W, Guardiola C, Juchaux M, Labiod D, Dendale R, Jourdain L, Sebrie C and Pouzoulet F 2017 Proton minibeam radiation therapy spares normal rat brain: Long-Term Clinical, Radiological and Histopathological Analysis *Sci. Rep.* 7 14403

Sayah R 2012 Evaluations des doses dues aux neutrons secondaires reçues par des patients de différents âges traités par protonthérapie pour des tumeurs intracrâniennes

Sayah R, Donadille L, Aubé A, Hérault J, Delacroix S, De Marzi L, Stichelbaut F and Clairand I 2013 Monte Carlo simulation of a proton therapy beamline for intracranial treatments *Radioprotection* **48** 317–39

Sayah R, Farah J, Donadille L, Hérault J, Delacroix S, De Marzi L, De Oliveira A, Vabre I, Stichelbaut F, Lee C, Bolch W E and Clairand I 2014 Secondary neutron doses received by paediatric patients during intracranial proton therapy treatments *J. Radiol. Prot.* **34** 279–86

Wellisch J P, Folger G and Ivanchenko V N 2005 The binary cascade *Monte Carlo 2005 Topical Meeting* pp 449–61

Wright D H and Kelsey M H 2015 The Geant4 Bertini Cascade *Nucl. Instruments Methods Phys. Res. Sect. A Accel. Spectrometers, Detect. Assoc. Equip.* **804** 175–88

Yeom Y S, Kuzmin G, Griffin K, Mille M, Polf J, Langner U, Jung J W, Lee C, Ellis D, Shin J and Lee C 2020 A Monte Carlo model for organ dose reconstruction of patients in pencil beam scanning (PBS) proton therapy for epidemiologic studies of late effects *J. Radiol. Prot.* **40** 225–42

Zacharatou Jarlskog C, Lee C, Bolch W E, George Xu X, Paganetti H and Med Biol Author manuscript P 2008 Assessment of organ specific neutron equivalent doses in proton therapy using computational whole-body age-dependent voxel phantoms NIH Public Access Author Manuscript *Phys Med Biol* **53** 693–717

Zanini A, Durisi E, Fasolo F, Visca L, Ongaro C, Nastasi U, Burn K W and Annand J R M 2004 Neutron spectra in a tissue equivalent phantom during photon radiotherapy treatment by LINACS *Radiat. Prot. Dosimetry* **110** 157–60